JOURNAL OF THEORETICAL AND APPLIED MECHANICS
44, 2, pp. 405-420, Warsaw 2006

NUMERICAL INVESTIGATION OF TRANSITIONAL FLOW IN CO- AND COUNTER-ROTATING ANNULAR CAVITY

Ewa Tuliszka-Sznitko
Artur Zieliński

Institute of Thermal Engineering, Technical University of Poznań
e-mail: sznitko@sol.put.poznan.pl

A 3D direct numerical simulation is performed to study the transitional flow in co- and counter-rotating annular cavity of the aspect ratio 5. The identification and characterization of mechanisms related to the laminar-turbulent process in rotating cavities should improve the prediction methods and lead to new, more effective boundary layer control strategies. Numerical computations are based on the pseudo-spectral Chebyshev-Fourier method for solving the incompressible Navier-Stokes equation. The numerical computations allow one to describe the steady axisymmetric basic state and 3D instability structures which appear in the transitional flow. The DNS computations are interpreted in the light of our LSA results. Moreover, the absolute instability regions are theoretically identified and the critical Reynolds numbers of the convective/absolute transition in both layers are given.

Key words: laminar-turbulent transition, rotating cavity, direct method

1. Introduction

The flow in rotating disk systems is not only a subject of fundamental interest but it is also a topic of practical importance. Typical configurations include cavities between rotating compressor and turbine disks. Numerous works have been recently devoted to the investigation of instabilities associated with flows past single and differentially rotating disks, Serre *et al.* (2001, 2004), Lingwood (1997), Tuliszka-Sznitko and Soong (2000), Tuliszka-Sznitko *et al.* (2002), Itoh (1991). For high rotation rates, flow in a rotor/stator cavity consists of two boundary layers of the Ekman type on the rotating disk and of the Bödewadt type on the stationary disk, separated by an inviscid rotating core. The transition process in both layers is related to type I and type II

generic linear instabilities. Type I instability is the inviscid instability. The mechanism of type II instability is related to combined effects of Coriolis and viscous forces. The instability structures in the rotating cavity were investigated numerically and experimentally by Dijkstra and van Heijst (1983), Szeri *et al.* (1983), Serre *et al.* (2001, 2004), Lopez *et al.* (2002), Gauthier *et al.* (2002), Schouveiler (1999, 2002) and others. The stability of the counter-rotating disk cavity of the aspect ratio $L > 10$ was studied by Szeri *et al.* (1983). The authors reported the existence of cylindrical and spiral vortices in boundary layers with the core itself remaining stable. Experimental investigations on instability of the co- and counter-rotating cylindrical cavity ($L = 20.9$) were also carried out by Gauthier *et al.* (2002). For the counter-rotating case, Gauthier has found a new instability pattern, which he called negative spirals.

Non-isothermal flow conditions were also considered (Mochizuki *et al.*, 1983; Tuliszka-Sznitko and Soong, 2000; Soong 1996), showing that thermal effects and the rotation-induced buoyancy become influential on stability characteristics and on critical conditions.

In the present paper, three-dimensional direct numerical calculations are performed for the annular co- and counter-rotating cavity of the aspect ratio $L = 5$ and curvature parameters $Rm = 1.5$ and 3.0. We study spatial structures which appear in boundary layers of both disks as well as the time dependence of these flows. Theoretical investigations (LSA) are also performed in order to enlighten the DNS results with respect to I and II instabilities. The geometrical and mathematical models are described in Section 2. The DNS and LSA numerical solution techniques are described in Sections 3 and 4, respectively. In Sections 5 and 6, the results obtained from DNS methods are analyzed. The theoretically identified absolute instability regions are discussed in Section 7.

2. Geometrical model, physical parameters and equations (DNS)

The geometrical model is a co- and counter-rotating cavity (Fig. 1). The outer cylinder of radius R_1, is attached to the stationary or slower rotating disk. The inner one of radius R_0 is attached to the faster rotating disk. The faster rotating disk rotates at a uniform angular velocity $\boldsymbol{\Omega}_1 = \Omega_1 \boldsymbol{e}_z$, where $\boldsymbol{e}_z$ is the unit vector. The slower rotating disk rotates at a angular velocity $\boldsymbol{\Omega}_2 = s\boldsymbol{\Omega}_1$. Positive s means that both disks rotate in the same direction and negative s means that disks rotate in opposite directions. The flow is controlled by the following physical parameters: the Reynolds number based

on the external radius of the disks and on the angular velocity of faster rotating disk Ω_1, $Re = R_1^2\Omega_1/\nu$, the local Reynolds number $Re_\delta = r^*/\delta = \sqrt{r^{*2}\Omega/\nu}$, the aspect ratio $L = (R_1 - R_0)/2h$ and the curvature parameter $Rm = (R_1 + R_0)/(R_1 - R_0)$. In the present study, calculations are performed for $L = 5$, $Rm = 3.0$ and 1.5 and for s from -0.2 to 0.5.

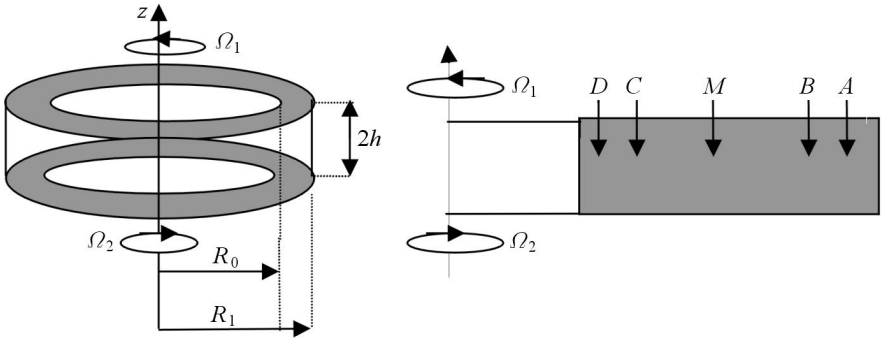

Fig. 1. Schematic picture of the rotating cavity

The governing equations are 3D Navier-Stokes equations, written in a velocity-pressure formulation together with the continuity equation

$$\frac{\partial \boldsymbol{V}}{\partial t} = \frac{1}{\mathrm{Re}}\Delta \boldsymbol{V} - (\boldsymbol{V}\cdot\nabla)\boldsymbol{V} - \nabla p \qquad \nabla\cdot\boldsymbol{V} = 0 \tag{2.1}$$

The equations are written in a cylindrical polar coordinate system (r, z, φ) with respect to a stationary frame of reference. In equation (2.1) t is time, p is pressure, $\boldsymbol{V}$ is the velocity vector and u, w, v are velocity components in the r, z, and φ directions, respectively. The time, space and velocity are normalized as follows: Ω_1^{-1}, h and $\Omega_1 R_1$. The dimensionless axial co-ordinate is $z = z^*/h$; $z \in [-1, 1]$ (asterisks denote dimensional values). The radius co-ordinate is additionally normalized in order to obtain the domain $[-1, 1]$ requested by the used spectral method, based on the Chebyshev polynomials: $r = (2r^* - (R_1 + R_0))/(R_1 - R_0)$.

No slip boundary condition is applied to all rigid walls, so $u = w = 0$. For the azimuthal velocity component, the boundary conditions are $v = (Rm + r)/(Rm + 1)$ on the top faster rotating disk, and $v = s(Rm + r)/(Rm + 1)$ on the slower rotating disk. However, because of the singularity of the azimuthal velocity component at the junction between the slower rotating disk and the inner end-wall, and between the faster rotating disk and the outer end-wall, these boundary conditions must be modified. The singularity express a physical situation in which there is a gap, for

instance, between the edge of the rotating disk and stationary end-wall. To eliminate these singularities, we used the following exponential profiles along the end-walls $r = \pm 1$:

a) end-wall attached to the stator
$v = [(Rm + r)/(Rm + 1)](1 - s)\exp[(z - 1)/0.006 + s]$

b) end-wall attached to the rotor
$v = [(Rm + r)/(Rm + 1)](1 - s)\{1 - \exp[(-z - 1)/0.006] + s\}$

Computations start with a sufficiently low Reynolds number Re=2000 to obtain a stable flow. The solution is then used as the initial condition for computation at a higher Reynolds number, with the small increment 500. We start the process of consecutively increased Re with the zero meridional flow and a linear distribution of the azimuthal velocity component.

3. Numerical approach (DNS)

The numerical solution is based on a pseudo-spectral collocation Chebyshev-Fourier-Galerkin approximation. The approximation of the flow variables $\Psi = (u, w, v, p)$ is given by an expansion into a truncated series (Serre *et al.*, 2001)

$$\Psi_{NMK}(r, z, \varphi, t) = \sum_{p=K/2}^{K/2-1} \sum_{n=0}^{N} \sum_{m=0}^{M} \widehat{\Psi}_{nmp}(t) T_n(r) T_m(z) \mathrm{e}^{\mathrm{i}p\varphi} \qquad \begin{matrix} -1 \leqslant r, z \leqslant 1 \\ 0 \leqslant \varphi \leqslant 2\pi \end{matrix} \tag{3.1}$$

where N, M and K are the numbers of collocation points in the radial, axial and azimuthal directions, respectively. $T_n(r) = \cos(n \arccos r)$ and $T_m(z) = \cos(m \arccos z)$ are Chebyshev polynomials, $\varphi_k = 2\pi k/K$, $k = 0, 1, 2, \ldots, K - 1$. Computations were performed for $N = 79$, $M = 49$ and $K = 95$. The time scheme is semi-implicit and second-order accurate. It corresponds to a combination of the second-order backward differentiation formula for the viscous diffusion term, and the Adams-Bashforth scheme for the non-linear terms. The method uses a projection scheme to maintain the incompressibility constraint. More information the reader can find in papers by Serre *et al.* (2001, 2004).

The behavior of the dependent variables is monitored at 15 points, in five different positions in the radial direction N (1/6, 1/3, 1/2, 2/3, 5/6) and in three positions in the axial direction M (9/10, 1/2, 1/10); Fig. 1.

4. Linear stability analysis (LSA)

The LSA computations were performed for the cylindrical rotor/rotor and rotor/stator cavity of an infinite radius. The disturbance equations were obtained by expressing the velocity and pressure fields as superposition of the basic state and perturbation field. A similarity model of the flow was used for generation of axially symmetric solutions of the basic state (Tuliszka-Sznitko and Soong, 2000; Tuliszka-Sznitko *et al.*, 2002).

We assume that the perturbation quantities have the following normal-mode form

$$[u', v', w', p']^\top = [\widehat{u}, \widehat{v}, \widehat{w}, \widehat{p}]^\top \exp(\alpha^* r^* + m\varphi - \omega^* t^*) + cc \tag{4.1}$$

where $\widehat{u}$, $\widehat{w}$, $\widehat{v}$ are the dimensional amplitudes of the three components of velocity in the radial, axial and azimuthal directions, respectively, $\widehat{p}$ is pressure, α^* and $\beta^* = m/r^*$ are the dimensional components of the wave number k^* in the radial and azimuthal directions, respectively, ω^* is the dimensional frequency and t^* is time. The co-ordinate system is located on the disk under consideration. The linear stability equations plus the homogeneous boundary conditions ($\widehat{u}(z^*) = \widehat{v}(z^*) = \widehat{w}(z^*) = \widehat{\tau}(z^*) = 0$ at $z^* = 0$ and $z^* = 2h$) constitute an eigenvalue problem which is solved in a global manner (Tuliszka-Sznitko and Soong, 2000; Tuliszka-Sznitko *et al.*, 2002). As in the DNS computations, a spectral collocation method based on Chebyshev polynomials is used for discretization of the LSA equations. The LSA is used to determine the absolute/convective character of the boundary layer in the rotating cavity.

5. Basic state

In this Section we analyze the basic state obtained from the DNS computations for $L = 5$, $Rm = 3.0$, 1,5 and for s ranging from -0.2 to 0.5. The basic state solution is steady and axisymmetric. Figures 2a,b,c show the velocity field in the meridional section $(r^*/h, z^*/h, 0.0)$, obtained for $s = 0.5$ (Re = 94000), $s = 0.0$ (Re = 26000) and $s = -0.2$ for (Re = 2250). From Fig. 2a and Fig. 2b, we can see that the fluid is pumped radially outward along the faster rotating disk (the upper one) and radially inward along the slower rotating disk. For an arbitrary positive and small negative rotational rate s, the flow is roughly the same as in the rotor-stator case: the flow consists of two disjoint boundary layers on each disk and of the central core flow. For

larger negative value of s (for instance $s = -0.2$), the flow is organized in a two-cell structure. The centrifugal flow, induced by rotation of the upper disk, recirculate along the bottom disk towards the inner end-wall. This inward flow meets the outward radial flow, induced by the rotation of the bottom disk, leading to creation of a stagnation area where the radial component of velocity vanishes.

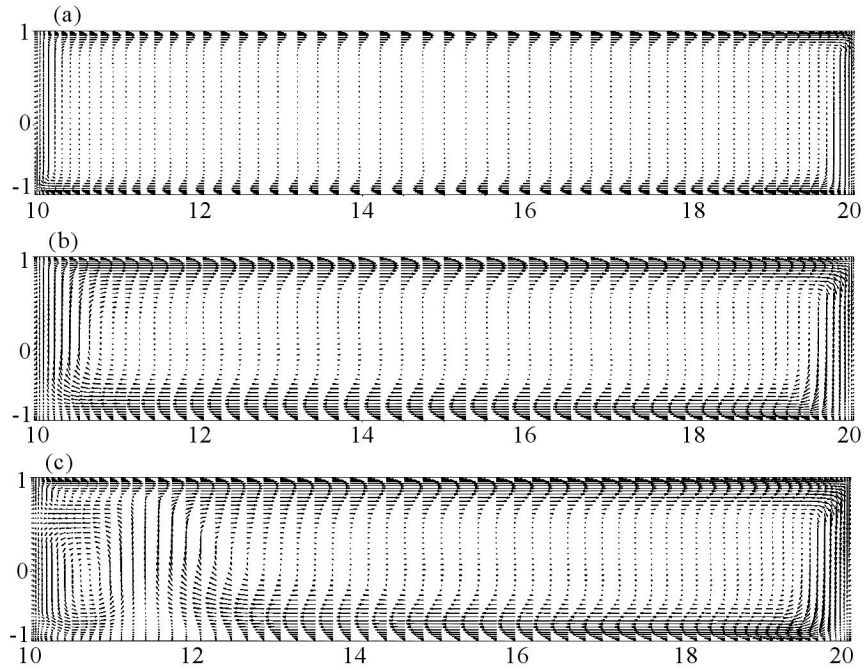

Fig. 2. The velocity field in the plane $(r^*/h, z^*/h, 0.0)$ obtained for: (a) $s = 0.5$ (Re = 94000), (b) $s = 0.0$, (Re = 26000), (c) $s = -0.2$ for (Re = 22500); $L = 5$, $Rm = 3.0$; DNS

From Fig. 2, we can see that the thickness of the bottom boundary layer for $s = -0.2$ and $s = 0.0$ clearly depends on the radius. The bottom disk boundary layer becomes more horizontal for the co-rotating case, $s = 0.5$. The dimensionless thickness of the bottom boundary layer $\delta^*/(\nu/\Omega)$ in terms of r^*/h, obtained for different s and Re, is illustrated in Fig. 3. For $s = -0.2$, the bottom disk boundary layer only exists for a larger radius; the thickness of the boundary layer increases towards the inner cylinder rapidly and finally reaches the upper disk boundary layer (at $r^*/h \sim 12$, Fig. 2c). At a slightly smaller $r^*/h \sim 11.6$, the stagnation area appears.

The two cell recirculating structure was investigated by Dijkstra and van Heijst (1983), Gauthier *et al.* (2002) and others.

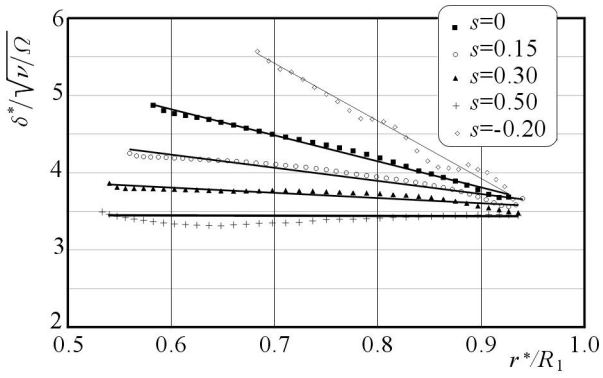

Fig. 3. Boundary layer thickness $\delta/\sqrt{\nu/\Omega_1}$ of the slower rotating disk in terms of the radial position r^*/R_1 obtained for $s = 0.5$ (Re = 94000), $s = 0.3$ (Re = 44000), $s = 0.15$ (Re = 34000), $s = 0.0$ (Re = 26000) and $s = -0.2$ for (Re = 22400); $L = 5$, $Rm = 3.0$, DNS

6. Instability structures

For all considered cases, we have found the same instability patterns in the stationary or slower rotating disk's boundary layer. With a fixed s, we increased Re, and over a certain Reynolds number we observed propagating cylindrical vortices in the slower rotating disk. Cylindrical vortices (2D), interpreted as type II instability, appear in the middle area of the boundary layer of the slower rotating disk and propagate towards the inner end-wall. Above the second critical value of Re, 3D spiral structures appear in the area near the outer end-wall. The spiral vortices, interpreted as type I instability, are observed for higher r^*/h. Gauthier *et al.* (2002) called these spirals "positive vortices" since they roll up to the centre in the direction of the faster rotating disk. These spiral vortices were studied extensively in the rotor-stator configuration among others by Schouveiler *et al.* (1999, 2002).

In Fig. 4 the isolines of the azimuthal velocity component disturbances, in the azimuthal section $(r^*/h, z^*/h = -0.95, \varphi)$ and in the meridional section $(r^*/h, z^*/h, \varphi = 0)$ obtained for Re = 27000, Re = 30000, Re = 50000, respectively, are presented $(s = 0.0, L = 5, Rm = 3.0)$. We can see that for Re = 27000 the cylindrical vortices co-exist with the spiral vortices. We observe two pairs of cylindrical waves and 19 spiral vortices. For higher Reynolds

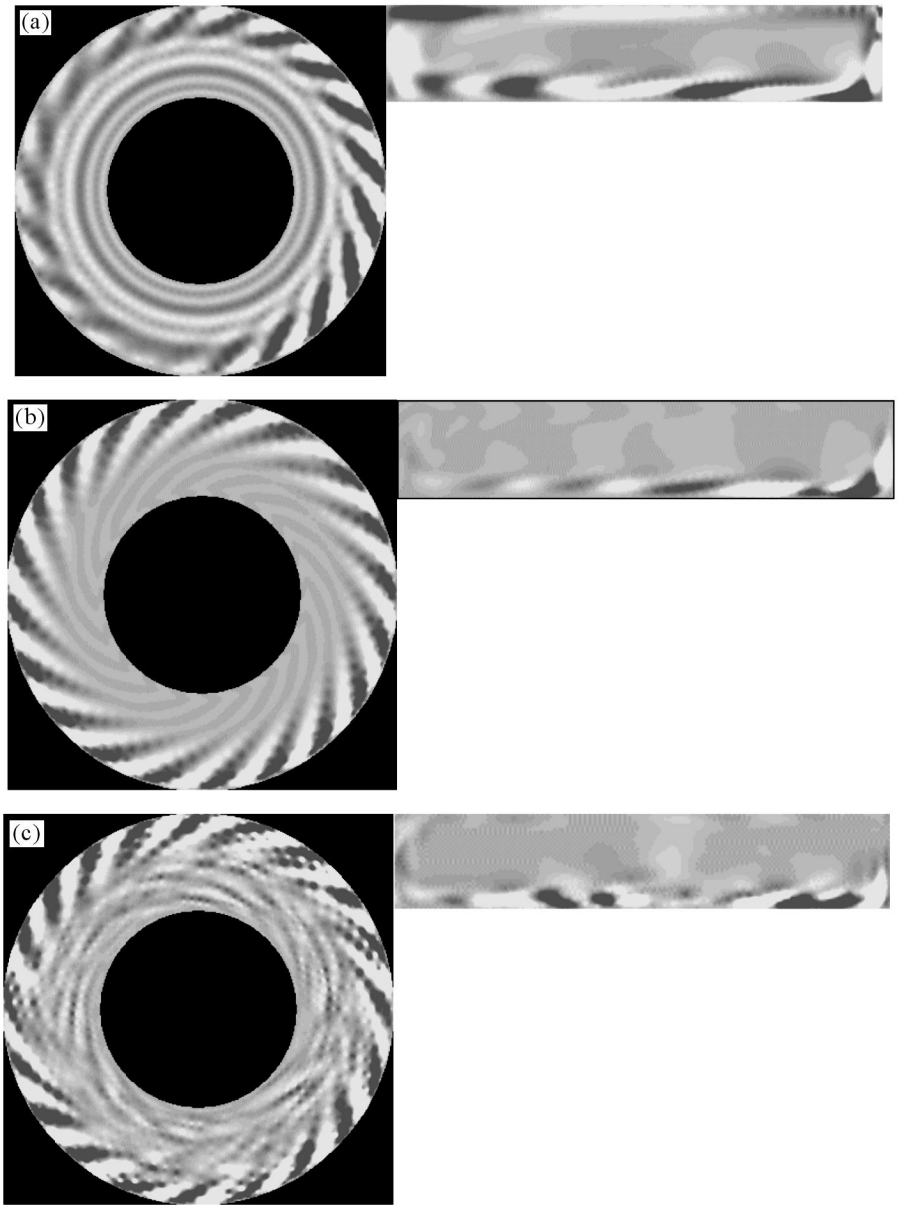

Fig. 4. Isolines of azimuthal velocity component disturbances in the azimuthal section $(r^*/h, z^*/h = -0.95, \varphi)$ and in the meridional section $(r^*/h, z^*/h, \varphi = 0)$ obtained for $\mathrm{Re} = 27000$, $\mathrm{Re} = 30000$, $\mathrm{Re} = 50000$, $s = 0$, $L = 5$, $Rm = 3.0$; DNS

numbers (Fig. 4b), type I instability is fully dominant. For consequently increasing Re, the flow becomes more and more disordered. We can notice that the turbulence starts from the inner end wall (Fig. 4c).

An exemplary instability characteristic of the azimuthal velocity component, obtained in the monitored point M in the stator boundary layer for $\mathrm{Re} = 30000$ is presented in Fig. 5. The obtained solution is oscillatory and has the angular frequency $\sigma = 2\pi/T = 1.9$, where T is the period of oscillation. For $L = 5$, $Rm = 3.0$, $s = 0.0$, the transition to unsteadiness is supercritical.

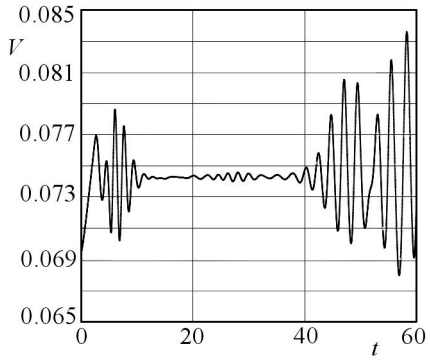

Fig. 5. The instability characteristic of the azimuthal velocity component obtained in the monitored point M in the stator boundary layer. $L = 5$, $Rm = 3.0$, $s = 0$, $\mathrm{Re} = 30000$; DNS

For the co-rotating cases, the critical Reynolds number of the transition to unsteadiness increased from $\mathrm{Re} = 27000$ for $s = 0$ up to 98000 for $s = 0.5$. For the counter-rotating case, the flow is significantly more unstable than for the rotor-stator case. For $s = -0.2$, the critical Reynolds number of transition to unsteadiness equals 23500. The influence of s on the critical Reynolds number of transition to unsteadiness is presented in Fig. 6.

The instability pattern obtained for the considered negative values of s in the bottom disk's boundary layer is the same as for the rotor-stator and co-rotating flow. Figure 7a shows isolines of azimuthal velocity component disturbances in the azimuthal plane $(r^*/h, z^*/h = -0.95, \varphi)$ obtained at $\mathrm{Re} = 24000$, $Rm = 3.0$, $L = 5$ and $s = -0.2$. As in the rotor-stator cavity $(s = 0.0)$, also for $s = -0.2$ we obtained 19 spiral vortices and two pairs of cylindrical vortices. The isolines of axial velocity component disturbances in the meridional section $(r^*/h, z^*/h, \varphi = 0)$ are presented in Fig. 7b. We can see from Fig. 7b that in the inner end-wall area, the structures fill the whole cell. The instability structures in the boundary layers of the slower rotating disk are observed for $r^*/h > 12.5$. The instability characteristic of the azimuthal

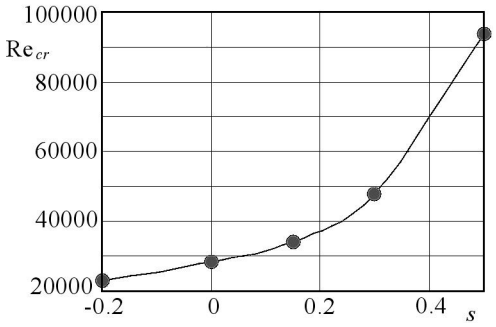

Fig. 6. The critical Reynolds number of transition to unsteadiness in terms of s; $L = 5$, $Rm = 3$; DNS

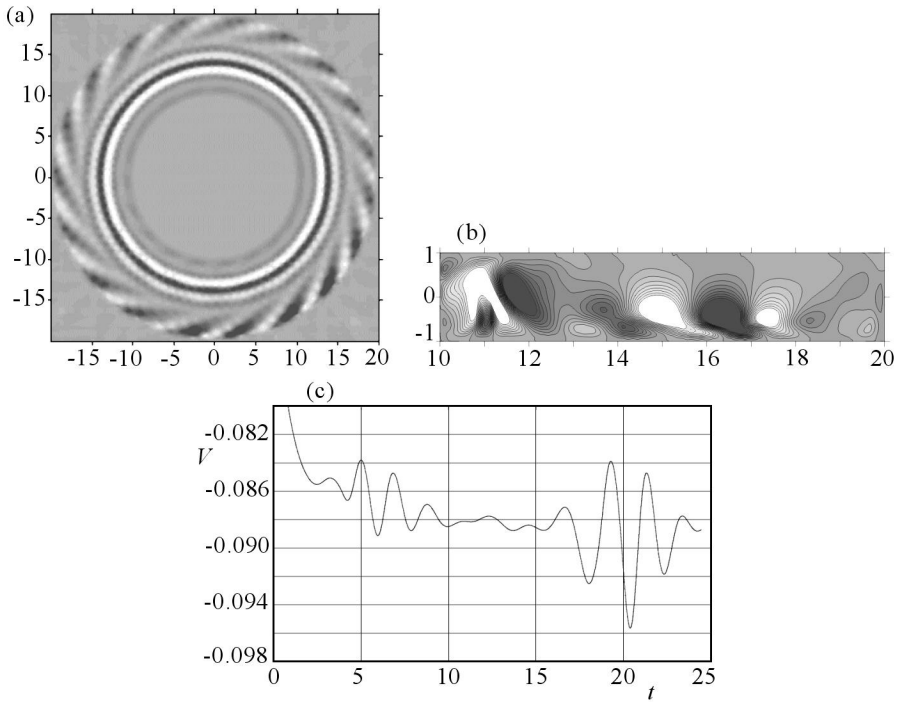

Fig. 7. Isolines of azimuthal velocity component disturbances in the $(r^*/h, z^*/h = -0.95, \varphi)$ plane (a), isolines of axial velocity component disturbances in the meridional plane $(r^*/h, z^*/h, \varphi = 0.0)$ (b), instability characteristics of the azimuthal velocity component obtained in the monitored point M (c), Re = 24000, $L = 5$, $Rm = 3.0$, $s = -0.2$; DNS

velocity component, obtained in the monitored point M in the stator boundary layer $(L = 5, Rm = 3.0, s = -0.2)$, is presented in Fig. 7c. The angular frequency of oscillations is equal to $\sigma = 2\pi/T = 2$.

For $Rm = 1.5$, $L = 5$, we obtained similar instability structures as for $Rm = 3.0$, $L = 5$. We observed two cylindrical and twelve spiral vortices. Exemplary isolines of azimuthal velocity component disturbances in the $(r^*/h, z^*/h = -0.95, \varphi)$ plane and isolines of axial velocity component disturbances in the $(r^*/h, z^*/h, \varphi = 0.0)$ plane, obtained for $s = 0$, $\mathrm{Re} = 26000$, are presented in Fig. 8a and Fig. 8b, respectively.

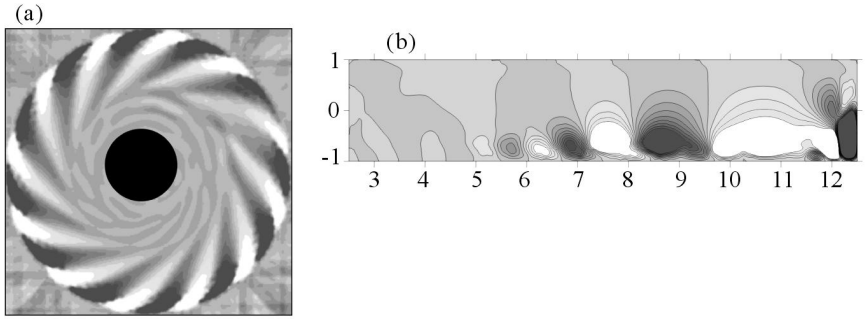

Fig. 8. Isolines of fluctuations of the axial velocity component at $\mathrm{Re}_R = 26000$, $Rm = 1.5$, $L = 5$, $s = 0.0$, (a) azimuthal plane $(r^*/h, z^*/h = -0.95, \varphi)$, (b) meridional plane $(r^*/h, z^*/h, \varphi = 0.0)$; DNS

We want to emphasize that the results were obtained for the inner end-wall attached to the faster rotating disk and the outer one attached to the slower rotating disk. This configuration was chosen because it was the most unstable. Our computations showed that the end-wall boundary conditions strongly influence the instability of boundary layers.

7. Absolute instability

The LSA results (Tuliszka-Sznitko and Soong, 2000) showed the existence of absolutely unstable areas in both stationary and rotating disk boundary layers of cylindrical rotor/stator cavities, with the critical local Reynolds numbers equal to $\mathrm{Re}_{\delta ca} = r^*/\delta = \sqrt{r^{*2}\Omega/\nu} = 48.5$ and $\mathrm{Re}_{\delta ca} = 562$, respectively. In Tuliszka-Sznitko and Soong (2000), the Briggs (1964) criterion was used to determine the regions of absolute instability. The critical Reynolds numbers of type II instability in the rotor and stator boundary layers were established at

$\mathrm{Re}_{\delta cII} = 90.23$ and 35.5, respectively. The critical Reynolds number of type I instability in the boundary layer of the rotating disk equaled $\mathrm{Re}_{\delta cI} = 278.6$. The critical Reynolds number of absolutely unstable area $\mathrm{Re}_{\delta ca} = 48.5$, in the boundary layer of the stationary disk, was very close to the critical Reynolds number of the convectively unstable area $\mathrm{Re}_{\delta cI} = 47$ (type I). The LSA results (Tuliszka-Sznitko and Soong, 2000) showed that almost the whole convectively unstable area in the boundary layer of the stationary disk, was absolutely unstable.

Animations of the spatio-temporal behavior of the disturbances, generated by the obtained DNS results, showed that type II and I structures propagate in the boundary layer of the stationary disk in the opposite directions. Cylindrical disturbances (type II) propagate towards the inner end-wall in accordance with the direction of the basic state flow, whereas type I structures propagate in the opposite direction towards the outer end-wall. This behavior could suggest (in accordance with the LSA results) that the area of dominance of type I instability in the stator boundary layer may be absolutely unstable.

To complete our previous LSA computations obtained for the rotor/stator cavity (Tuliszka-Sznitko and Soong, 2000), we performed LSA computations for co-rotating rotor/rotor configurations. We found that the critical local Reynolds number of type I instability increases in the slower rotating disk from $\mathrm{Re}_{\delta cI} = 47$ for $s = 0.0$ to $\mathrm{Re}_{\delta cI} = 770$ for $s = 0.75$ and in the faster rotating disk from $\mathrm{Re}_{\delta cI} = 278.6$ to $\mathrm{Re}_{\delta cI} = 930$. The critical Reynolds number of type II instability increases in the slower rotating disk from $\mathrm{Re}_{\delta cII} = 35.5$ for $s = 0.0$ to $\mathrm{Re}_{\delta cII} = 405$ for $s = 0.75$ and in the faster rotating disk from $\mathrm{Re}_{\delta cII} = 90.23$ to $\mathrm{Re}_{\delta cII} = 419$. These results are in good agreement with Itoh (1991). We also observed rapid increase in the critical Reynolds number of the absolutely unstable area with increasing s in both boundary layers; for the faster rotating disk it increases from $\mathrm{Re}_{\delta ca} = 562$ for $s = 0.0$ to $\mathrm{Re}_{\delta ca} = 1685$ for $s = 0.75$. Exemplary neutral curves in the plane $(\sigma, \mathrm{Re}_\delta)$ obtained for $s = 0.0$, 0.5, 0.75 and 0.9 in the boundary layer of the faster rotating disk are presented in Fig. 9. The critical local Reynolds numbers $\mathrm{Re}_{\delta cI}$, $\mathrm{Re}_{\delta cII}$ and $\mathrm{Re}_{\delta ca}$ in terms of s obtained for the faster rotating disk are presented in Fig. 10. From Fig. 9 and Fig. 10, we can see that with increasing s the flow becomes more and more stable, and the absolutely unstable flow vanishes. These LSA results are in good agreement with our DNS results presented in Fig. 6 where we observe a rapid increase in the critical Reynolds number of transition to unsteadiness with increasing s.

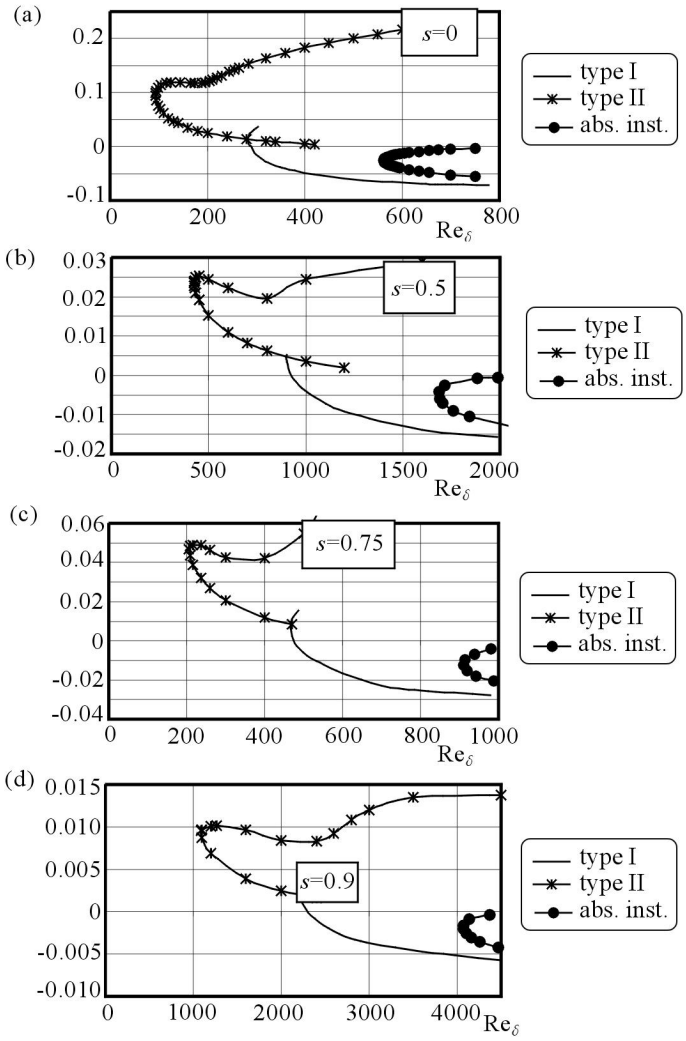

Fig. 9. Exemplary neutral curves in the plane $(\sigma, \mathrm{Re}_{\delta I})$ obtained for $s = 0.0$, 0.5, 0.75 and 0.9 in the faster rotating disk; LSA

8. Conclusions

An incompressible 3D fluid flow between co- and counter-rotating disks with enclosing inner and outer cylinders attached to faster and slower rotating disks, respectively, was investigated numerically using the DNS method. We

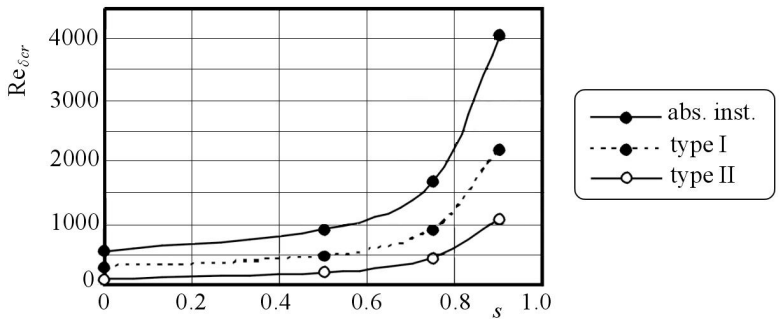

Fig. 10. Critical local Reynolds numbers $\mathrm{Re}_{\delta cI}$, $\mathrm{Re}_{\delta cII}$ and $\mathrm{Re}_{\delta ca}$ in terms of s obtained for the boundary layer of the faster rotating disk; LSA

investigated an annular cavity of the aspect ratio $L = 5$ and $Rm = 1.5$, 3.0. The computations showed complexity of the flow. In the stationary or, slower rotating disk's boundary layer two different patterns of instability structures were observed and described: two-dimensional vortices propagating towards the inner end-wall along the slower rotating disk and three-dimensional spiral vortices propagating in the opposite direction. We analyzed the counter-rotating computations in the light of Gauthier's *et al.* (2002) experimental results, obtained for a cylindrical cavity of the aspect ratio $L = 20.9$. We received the same structure of the basic state with a stagnation circle in which the radial component of the velocity vanishes.

The animation of the flow, based on the obtained DNS results, showed that type II instability structures in the boundary layer of the stationary disk propagate downstream towards the inner end-wall, whereas type I propagates in the opposite direction (up-stream). It could possibly indicate (in accordance with previous LSA results, see Tuliszka-Sznitko and Soong, 2000) that partly the stator boundary layer may be absolutely unstable. Our present LSA computation carried out for a co-rotating rotor/rotor cavity proved that with increasing s the flow becomes more and more stable and the absolutely unstable area slowly vanishes.

Acknowledgements

The computations were carried out at the Supercomputing and Networking Center in Poznań within the framework of the KBN grant 4T07 A04528 supported by the State Committee for Scientific Research.

References

1. BRIGGS R.J., 1964, *Electron-Steam Interaction with Plasmas*, Chap. 2, MTT Press
2. DIJKSTRA D., VAN HEIJST G., 1983, The flow between finite rotating discs enclosed by a cylinder, *J. Fluid Mech.*, **128**, 123, 123-154
3. GAUTHIER G., GONDRET P., MOISY F., RABAUT M., 2002, Instabilities in the flow between co- and counter-rotating disks, *J. Fluid Mech.*, **473**, 1-21
4. ITOH M., 1991, On the instability of the flow between coaxial rotating disks, In: *Boundary Layer Stability and Transition to Turbulence, ASME FED*, **114**, 83
5. LINGWOOD R., 1997, Absolute instability of the Ekman layer and related rotating flows, *J. Fluid. Mech.*, **331**, 405, 405-428
6. LOPEZ J., HART J., MARQUES F., KITTELMAN S., SHEN J., 2002, Instability and mode interactions in a differentially driven rotating cylinder, *J. Fluid Mech.*, **462**, 383-409
7. MOCHIZUKI *et al.*, 1983, Heat transfer mechanisms and performance in multiple parallel disk assemblies, *Trans. ASME, J. Heat Transfer*, **105**, 598-604
8. OWEN J., ROGERS R., 1995, Heat transfer in rotating disc systems, In: *Rotating Cavity*, Vol. 2, W.D. Morris (edit.), Wiley
9. SCHOUVEILER L., LE GAL P., CHAUVE P., 2002, Instabilities of the flow between a rotating and stationary disk, *J. Fluid Mech.*, **443**, 329-350
10. SCHOUVEILER L., LE GAL P., CHAUVE P., TAKEDA Y., 1999, Spiral and circular waves in the flow between a rotating and a stationary disc, *Experiments in Fluids*, **26**, 179
11. SERRE E., CRESPO DEL ARCO E., BONTOUX J., 2001, Annular and spiral patters in flow between rotating and stationary disks, *J. Fluid. Mech.*, **434**, 65, 65-100
12. SERRE E., TULISZKA-SZNITKO E., BONTOUX P., 2004, Coupled numerical and theoretical study of the flow transition between a rotating and stationary disk, *Phys. of Fluids*, **16**, 3
13. SOONG C.Y., 1996, Theoretical analysis for axisymmetric mixed convention between rotating coaxial disks, *Int. J. Heat Mass Transfer*, **39**, 8, 1569-1583
14. SZERI A., GIRON A., SCHNEIDER S., KAUFMAN H., 1983, Flow between rotating disks, Part II. Stability, *J. Fluid Mech.*, **443**, 329-350
15. TULISZKA-SZNITKO E, SOONG C.Y., 2000, Instability of non-isothermal flow between coaxial rotating disks, *Proceedings of European Congress on Computational Methods in Applied Sciences and Engineering*, Barcelona

16. Tuliszka-Sznitko E., Serre E., Bontoux P., 2002, On the nature of the boundary layers instabilities in a flow between a rotating and a stationary disc, *C.R. Mecanique*, **30**, 90-99

Badanie przejścia laminarno-turbulentnego pomiędzy dyskami wirującymi w konfiguracji wirnik/wirnik

Streszczenie

W pracy badany jest metodą bezpośrednią przepływ nieściśliwy w przestrzeni pomiędzy dwoma wirującymi tarczami i dwoma wirującymi pierścieniami. Do obliczeń numerycznych zastosowano metodę spektralnej kolokacji bazującą na szeregach Czebyszewa i szeregu Fouriera. Obliczenia przeprowadzono dla współczynnika rozciągłości obszaru $L = 5$ i współczynnika krzywizny $Rm = 1.5$ i 3.0. Badania wykazały olbrzymią złożoność badanego przepływu i różnorodność struktur niestabilnościowych występujących w obszarze przejścia laminarno-turbulentnego. Badania bezpośrednie (DNS) uzupełnione zostały badaniami teoretycznymi (LSA), które umożliwiły między innymi wyznaczenia w przestrzeni pomiędzy wirującymi tarczami obszarów o niestabilności absolutnej.

Manuscript received August 31, 2005; accepted for print December 7, 2005